processes

MDPI

Article

The Effect of PVA Binder Solvent Composition on the Microstructure and Electrical Properties of $0.98BaTiO_3$-$0.02(Ba_{0.5}Ca_{0.5})SiO_3$ Doped with Dy_2O_3

Nak-Beom Jo, Jin-Seok Baek and Eung-Soo Kim *

Department of Advanced Materials Engineering, Graduate School, Kyonggi University, Suwon 16227, Korea; pilot3705@kyonggi.ac.kr (N.-B.J.); baekjs95@kyonggi.ac.kr (J.-S.B.)
* Correspondence: eskim@kyonggi.ac.kr; Tel.: +82-31-249-9764

Abstract: In this study, the effect of the polyvinyl alcohol (PVA) binder solvent composition on the electrical properties of sintered $0.98BaTiO_3$-$0.02(Ba_{0.5}Ca_{0.5})SiO_3$ ceramics doped with x wt.% Dy_2O_3 ($0.0 \leq x \leq 0.3$) was investigated. In the absence of the PVA binder, the specimens sintered at 1260 and 1320 °C for 1 h in a reducing atmosphere showed a single $BaTiO_3$ phase with the perovskite structure. The relative densities of the specimens were higher than 90%, and the grain morphologies were uniform for all the solvent compositions. At 1 kHz, the dielectric constant of the specimens depended not only on their crystal structural characteristics, but also on their microstructural characteristics. The microstructural characteristics of the specimens with the PVA binder were affected by the ethyl alcohol:water ratio of the 10 wt.% PVA-111 solution. A homogeneous microstructure was observed for the 0.1 wt.% Dy_2O_3-doped specimens sintered at 1320 °C for 1 h when the ethyl alcohol/water ratio of the binder solution was 40/60. These specimens showed the maximum dielectric constant (ε_r = 2723.3) and an insulation resistance of 270 GΩ. The relationships between the microstructural characteristics and dissipation factor (tanδ) of the specimens were also investigated.

Keywords: $BaTiO_3$-based ceramics; binder; MLCC; electrical properties

Citation: Jo, N.-B.; Baek, J.-S.; Kim, E.-S. The Effect of PVA Binder Solvent Composition on the Microstructure and Electrical Properties of $0.98BaTiO_3$-$0.02(Ba_{0.5}Ca_{0.5})SiO_3$ Doped with Dy_2O_3. *Processes* **2021**, *9*, 2067. https://doi.org/10.3390/pr9112067

Academic Editor: Sung-Churl Choi

Received: 22 October 2021
Accepted: 16 November 2021
Published: 18 November 2021

1. Introduction

The rapid progress in the development of novel electronic devices has increased the demand for miniaturisation and the development of high-efficiency and highly functional electronic components. With the electrification of automobiles, the research to improve the performance of passive components, such as capacitors, inductors, and resistors, has skyrocketed. Among the various passive devices investigated to date, multilayer ceramic capacitors have been extensively investigated owing to their high energy capacity per unit size, thermal stability, and high reliability [1–4].

$BaTiO_3$ ceramics are representative ferroelectric dielectrics with a perovskite structure and are used as the base material for capacitors. $BaTiO_3$ ceramics show several crystal structural phases depending on the displacement of ions constituting the unit lattice of the crystal structure. The most important structural characteristic of $BaTiO_3$ ceramics for capacitor applications is the tetragonality (c/a) of their lattice parameters. To improve the dielectric properties of $BaTiO_3$ ceramics, various dopant additives that can increase the dielectric constant (K) of these ceramics are investigated. This is because such dopants can increase the tetragonality and octahedral volume of the unit cell [5,6].

To realise the application of $BaTiO_3$-based ceramics for high-performance ceramic capacitors, it is important not only to improve their tetragonality, but also to control their microstructural uniformity. This is because the microstructural heterogeneity of the capacitor material reduces the reliability and capacitance of the entire electronic device.

In this study, $BaTiO_3$ ceramics with 0.02 mol of $(Ba_{0.5}Ca_{0.5})SiO_3$ were used as the base dielectric material. The addition of 2mol% $(Ba_{0.5}Ca_{0.5})SiO_3$ controlled the highly densified

microstructure of the specimens in the sintering step and improved the insulation resistance of the sintered specimens [7]. To investigate the substitutional effect of Dy^{3+} ions on the dielectric properties of the $BaTiO_3$-based ceramics, the Dy_2O_3 content of the specimens was varied from 0.0 to 0.3 wt.% to eliminate the effect of Dy_2O_3 as the secondary phase on the microstructural characteristics of the ceramics [8,9].

The electrical properties of sintered $BaTiO_3$-based ceramics are affected predominantly by their microstructural characteristics. Various organic additives are investigated to control the particle dispersion and/or uniform grain growth of $BaTiO_3$-based ceramics [10–12]. Among the various organic additives investigated to date, the polyvinyl alcohol (PVA) binder effectively suppresses the separation of powder due to the difference in the particle sizes and densities of the raw materials for $BaTiO_3$ and the oxide additives [13,14]. Although water is used as the solvent to disperse the PVA additive in ceramic powders, microstructural heterogeneities, such as pores, are observed in the specimens owing to the high surface tension of water. This deteriorates the dielectric properties of the specimens [15]. A mixed solution of water and ethyl alcohol as a hydrophilic solvent not only improves the dispersion of PVA, but also dissolves PVA [16] in ceramic powders, thus improving their microstructural homogeneity and electrical properties by controlling the characteristics of the binder solution.

In this study, to effectively control the electrical properties of $0.98BaTiO_3$-$0.02(Ba_{0.5}Ca_{0.5})SiO_3$ ceramics by achieving microstructural homogeneity, the composition of the PVA binder solvent containing ethyl alcohol and water was optimised.

2. Materials and Methods

2.1. Binder Solution Preparation

The solvent composition of the binder solution was optimised to improve the viscosity of the ceramic powder, increase the adhesion with binder solution, and improve the electrical properties of the ceramics. According to Khattab et al. [16], the viscosity of a mixture of 60 vol.% water and 40 vol.% ethyl alcohol is the highest at room temperature. In addition, to investigate the effect of the viscosity of the binder solvent on the electrical properties of $0.98BaTiO_3$-$0.02(Ba_{0.5}Ca_{0.5})SiO_3$, solvent compositions (2)–(5) in Table 1 were selected. Additional 10 wt.% of the solvent was added to the binder solution containing the raw material and solvent to improve the solubility of PVA-111 (99.9%, Sigma Aldrich, St. Louis, MO, USA) in the solution [17].

Table 1. Viscosity and surface tension values of the water-ethyl alcohol solutions with different compositions.

	Compositions	Chemical Formula	Density (g/cm^3)	Viscosity (Pa·s)	Surface Tension (N/m)
	PVA-111	$(R\text{-}CH_4O_4P)_n$(99.9%)	-	-	-
(1)	Water 100%	H_2O (99.9%)	0.9971	0.8914	71.97
(2)	Water 80 vol.% + ethyl alcohol 20 vol.%	-	0.9548	2.1009	32.17
(3)	Water 60 vol.% + ethyl alcohol 40 vol.%	-	0.9125	2.2208	29.63
(4)	Water 40 vol.% + ethyl alcohol 60 vol.%	-	0.8702	1.9780	25.78
(5)	Water 20 vol.% + ethyl alcohol 80 vol.%	-	0.8279	1.6345	24.10
(6)	Ethyl alcohol 100%	C_2H_5OH (99.9%)	0.7858	1.0740	22.27

The binder solution was prepared by adding 10 wt.% of PVA-111 to a mixture of distilled water and ethyl alcohol (99.9%, Samchun, Seoul, Republic of Korea) (water volume/ethyl alcohol volume = 4.00, 1.50, 0.67, 0.25). The compositions of the different binder solutions prepared in this study are listed in Table 2. The binder solution was homogenised

using a non-contact sonicator (SH-2300D, Saehan, Seoul, Republic of Korea) at 40 kHz and 65 °C for 1 h.

Table 2. Compositions of the binder solutions.

Type of Binder	Binder Solution Composition	Water Volume/ Ethyl Alcohol	Mixing Condition
Binder A	Water 80 vol.% + Ethanol 20 vol.% with 10 wt.% of PVA-111	4.00	(Sonicator) 40 kHz 65 °C 1 h
Binder B	Water 60 vol.% + Ethanol 40 vol.% with 10 wt.% of PVA-111	1.50	
Binder C	Water 40 vol.% + Ethanol 60 vol.% with 10 wt.% of PVA-111	0.67	
Binder D	Water 20 vol.% + Ethanol 80 vol.% with 10 wt.% of PVA-111	0.25	

2.2. Preparation of Sample

High-purity $BaTiO_3$ (170nm, 99.9%, Fuji Titanium Industry, Osaka, Japan), $(Ba_{0.5}Ca_{0.5})SiO_3$ glass frit powder (99.9%, NYG Co.,Ltd, Amagasaki, Japan) and Dy_2O_3 (99.9%, Solvey, Brussels, Belgium) powders were used as the starting materials for preparing the ceramics. The powders were weighed according to the composition of $BaTiO_3$ and Dy_2O_3 (x wt.%, $0.0 \leq x \leq 0.3$) in the ceramics. The mixed powders were ball-milled using yttrium-stabilised zirconia balls for 24 h in ethyl alcohol and dried. Subsequently, the dried powders were mixed with the 1 wt.% PVA binder solutions (binders A, B, C, and D in Table 2) and pressed isostatically into 15 mm-diameter disks at 1500 kg/cm^2. The pressed disks were sintered at 1260 and 1320 °C for 1 h in a reducing atmosphere (95% N_2 and 5% H_2) with flow rate (0.5L/min).

2.3. Evaluation of Physical and Electrical Properties

The apparent densities of the specimens were determined using the Archimedes method, and their theoretical densities were calculated from their XRD patterns. The relative densities of the specimens were calculated from their apparent and theoretical densities. The crystalline phases of the specimens were analysed using XRD (D/max–2500V/PC, Rigaku, Tokyo, Japan) over the 2θ range of 20–70°. Rietveld refinement measurements were performed on the XRD data method using Fullprof software (WinPLOTR) and the structural characteristics, such as the lattice parameters, atomic positions, and tetragonality, of the sintered specimens were analysed. SEM (SU-70/Horiba, Hitachi, Japan) was used to observe the microstructures of the specimens. Silver electrodes were attached to both the surfaces of the specimens by firing them at 520 °C for 10 min. The dielectric constants (K) of the specimens were calculated from their measured capacitances (nF) using an LCR meter (E4980A, Agilent, Santa Clara, CA, USA) at 1 kHz. The IR of the specimens was measured at 25°C using an insulation resistance meter (AT683, Applent Ins. Ltd., Chanzhou, China) at 500 V for 60 s.

3. Results and Discussion

3.1. Physical and Electrical Properties of the $0.98BaTiO_3$-$0.02(Ba_{0.5}Ca_{0.5})SiO_3$ Ceramics Doped with Dy_2O_3

3.1.1. Physical Properties

The X-ray diffraction (XRD) patterns of the Dy_2O_3-doped $0.98BaTiO_3$-$0.02(Ba_{0.5}Ca_{0.5})SiO_3$ ceramics sintered at 1260 and 1320 °C for 1 h are shown in Figure 1. A single phase of $BaTiO_3$ with the perovskite structure was observed for the ceramics sintered at 1320 °C for 1 h, irrespective of Dy_2O_3 content. According to Roy et al., 2mol% of $(Ba_{0.5}Ca_{0.5})SiO_3$ is sufficient to be dissolved in the $BaTiO_3$ lattice [18]. Therefore, $(Ba_{0.5}Ca_{0.5})SiO_3$ was not detected for the entire range of compositions. On the other hand, the specimens doped with more than 0.2 wt.% Dy_2O_3 and sintered at 1260 °C for 1 h showed a Dy_2O_3 secondary phase. This is because Dy^{3+} ions dissolve in the $BaTiO_3$ structure at temperatures higher than 1300 °C [19].

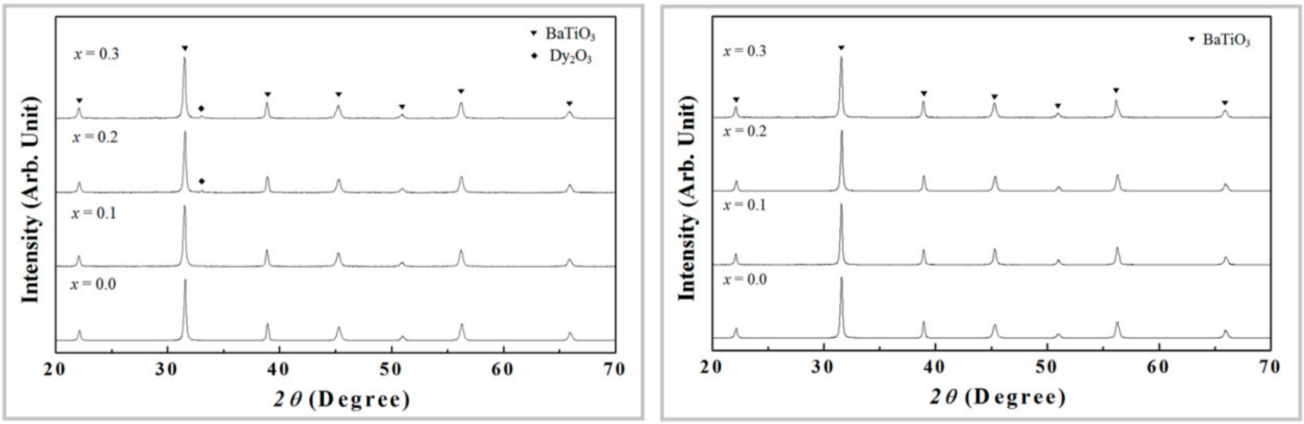

Figure 1. X-ray diffraction (XRD) patterns of the $0.98BaTiO_3$-$0.02(Ba_{0.5}Ca_{0.5})SiO_3$ ceramics doped with x wt.% Dy_2O_3 ($0.0 \leq x \leq 0.3$) and (**a**) sintered at 1260 °C for 1 h and (**b**) 1320 °C for 1 h.

Table 3 shows the relative densities of the sintered specimens with various Dy_2O_3 contents. The relative density of the sintered specimens increased with an increase in the Dy_2O_3 content because of the increase in the amount of Dy^{2+} ions dissolved in the $BaTiO_3$ structure. The relative density of the specimens sintered at 1260 °C for 1 h was 88.84–89.49%, while that of the specimens sintered at 1320 °C for 1 h was higher than 90%. Moreover, it is reported that if microstructural defects and/or pores are considered as the secondary phase, the dielectric behaviour of a ceramic can be well represented by the "Maxwell relationship" [20] for relative densities higher than 90% and represents a low dielectric constant according to the "Niesel equation" modified for the relative density [21].

Table 3. Relative densities of the $0.98BaTiO_3$-$0.02(Ba_{0.5}Ca_{0.5})SiO_3$ ceramics with different Dy_2O_3 additive contents without binder solution and sintering temperatures.

Composition	Sintering Condition	Density (g/cm^3)	Theoretical Density (g/cm^3)	Relative Density
$0.02(Ba_{0.5}Ca_{0.5})SiO_3$-$0.98BaTiO_3$	1260 °C 1 h	5.3418	6.0127	88.84%
	1320 °C 1 h	5.4324		90.35%
$0.02(Ba_{0.5}Ca_{0.5})SiO_3$-$0.98BaTiO_3$ with 0.1wt.%Dy_2O_3	1260 °C 1 h	5.3612	6.0133	89.16%
	1320 °C 1 h	5.4853		91.22%
$0.02(Ba_{0.5}Ca_{0.5})SiO_3$-$0.98BaTiO_3$ with 0.2wt.%Dy_2O_3	1260 °C 1 h	5.3739	6.0139	89.36%
	1320 °C 1 h	5.4421		90.49%
$0.02(Ba_{0.5}Ca_{0.5})SiO_3$-$0.98BaTiO_3$ with 0.3wt.%Dy_2O_3	1260 °C 1 h	5.3820	6.0144	89.49%
	1320 °C 1 h	5.4415		90.47%

3.1.2. Electrical Properties

The dielectric constants and dissipation factors (tanδ) of the Dy_2O_3–doped ($0.0 \leq x \leq 0.3$) and sintered $0.98BaTiO_3$-$0.02(Ba_{0.5}Ca_{0.5})SiO_3$ ceramics are shown in Figure 2. With an increase in the Dy_2O_3 content, the dielectric constant of the specimens increased, and the sintered specimens doped with 0.1 wt.% Dy_2O_3 showed the highest dielectric constant K of 1878.5, which decreased with a further addition of Dy_2O_3, as indicated by Figure 2. Dy^{3+} incorporation into Ti^{4+}-site of $BaTiO_3$ and the formation of oxygen vacancies can be expected by Equation (1).

$$2BaO + Dy_2O_3 \rightarrow 2Ba_{Ba} + 2Dy'_{Ti} + 5O_O + V^{\cdot\cdot}{}_O \quad (1)$$

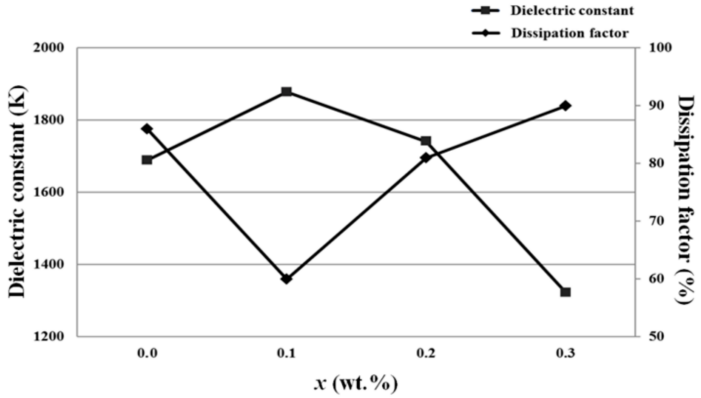

Figure 2. Dielectric constant and dissipation factor (tanδ) of the $0.98BaTiO_3$-$0.02(Ba_{0.5}Ca_{0.5})SiO_3$ ceramics doped with x wt.% of Dy_2O_3 ($0.0 \leq x \leq 0.3$) without binder solution and sintered at 1320 °C for 1 h.

These oxygen vacancies compensate for the charge reduction and reduce the dielectric loss by reducing the low electric field loss, which is the dielectric loss due to the 90° domain shift.

Therefore, the sintered specimens with 0.1 wt.% Dy_2O_3 showed the lowest dissipation factor (tanδ) of 0.605, which then increased because of the changes in the microstructural characteristics of the specimens, as indicated by Figure 3.

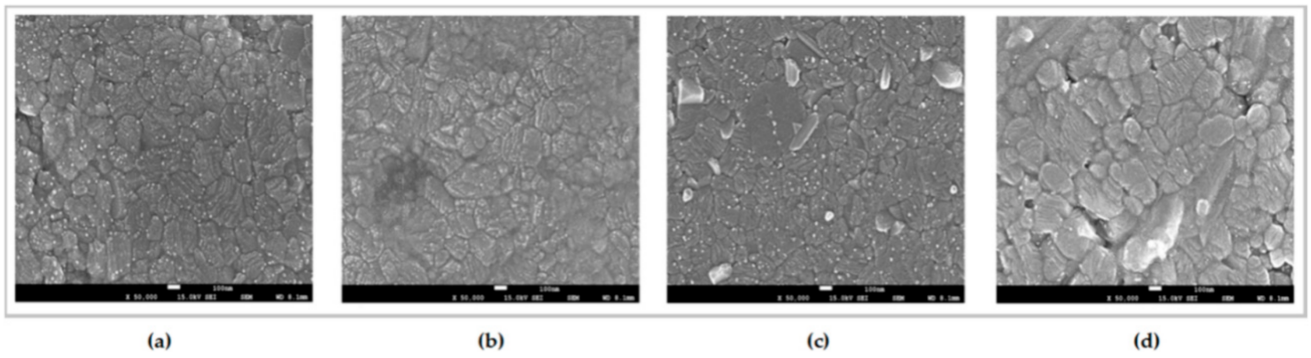

Figure 3. Scanning electron microscopy (SEM) images of the Dy_2O_3–doped $0.98BaTiO_3$ -$0.02(Ba_{0.5}Ca_{0.5})SiO_3$ ceramics sintered at 1320 °C for 1 h. (bar: 100 nm): (**a**) 0.0, (**b**) 0.1, (**c**) 0.2, (**d**) 0.3 wt.% Dy_2O_3.

The scanning electron microscopy (SEM) images of polished surface of the x wt.% Dy_2O_3–doped $0.98BaTiO_3$-$0.02(Ba_{0.5}Ca_{0.5})SiO_3$ ceramics ($0.0 \leq x \leq 0.3$) sintered at 1320 °C for 1 h are shown in Figure 3. Because the relative density of the specimens was higher than 90% for all the solvent compositions, dense and uniform grains were observed, and the grain size did not change significantly with the Dy_2O_3 content. However, with an increase in the Dy_2O_3 content, the number of microstructural defects, such as pores, increased, and finally, a decrease in the capacitance and an increase in the dissipation factor (tanδ) were observed owing to the decrease in the microstructural homogeneity of the sintered specimens doped with more than 0.1 wt.% Dy_2O_3. These results are consistent with the increase in the number of oxygen vacancies with an increase in the substitutional Dy^{3+} dopant ion concentration in $BaTiO_3$ [22,23]. Therefore, the Dy_2O_3-doped $0.98BaTiO_3$-$0.02(Ba_{0.5}Ca_{0.5})SiO_3$ ceramics sintered at 1320 °C for 1 h were further examined to investigate the effect of the microstructural characteristics of $BaTiO_3$-based ceramics on their electrical properties.

3.2. The Effect of the PVA Binder Solvent Composition on the Physical and Electrical Properties of the Ceramics

To effectively control the microstructural homogeneity and electrical properties of the 0.1 wt.% Dy_2O_3-doped $0.98BaTiO_3$-$0.02(Ba_{0.5}Ca_{0.5})SiO_3$ specimens sintered at 1320 °C for 1 h, the effect of the PVA binder solvent composition on the microstructure and electrical properties of the sintered specimens was investigated.

3.2.1. Physical Properties

Figure 4 shows the XRD patterns of the 0.1 wt.% of Dy_2O_3-doped $0.98BaTiO_3$-$0.02(Ba_{0.5}Ca_{0.5})SiO_3$ specimens sintered at 1320 °C for 1 h with different binders. The specimens showed the $BaTiO_3$ single phase with the perovskite structure, irrespective of the binder composition. Rietveld refinement was performed for the specimens sintered at 1320 °C for 1 h with different binder solutions to investigate the effect of the crystalline structural characteristics of the specimens on their electrical properties, as shown in Figure 5. The dotted lines represent the intensity of the XRD peaks, while the solid lines represent the calculated intensity. The bottom line denotes the difference between the observed and calculated values, and the refined plot showed high reliability. The crystalline structural parameters determined from the Rietveld refinement measurements are listed in Table 4. The goodness of fit value was within the range of 1.2–1.3, while the Bragg R-factor value ranged from 2.41 to 2.83 for all the binder compositions. These values confirm the formation of the tetragonal perovskite structure with the P4mm space group. No change was observed in the crystal structural parameters, such as the lattice parameter (a, b, c), unit cell volume and tetragonality, with the variation in the binder solution, as shown in Table 4.

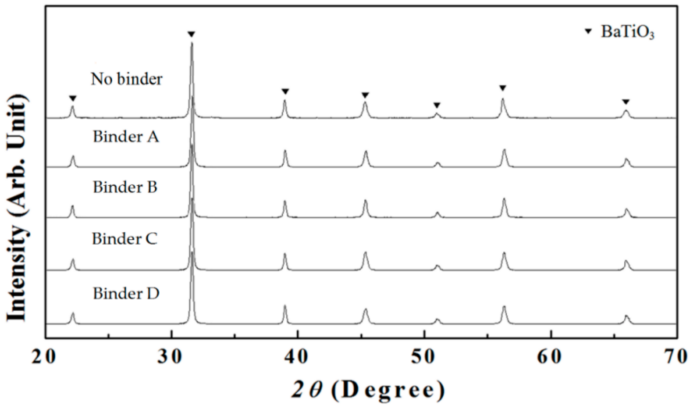

Figure 4. XRD patterns of the 0.1 wt.% Dy_2O_3-doped $0.98BaTiO_3$-$0.02(Ba_{0.5}Ca_{0.5})SiO_3$ ceramics sintered at 1320 °C for 1 h with different binders.

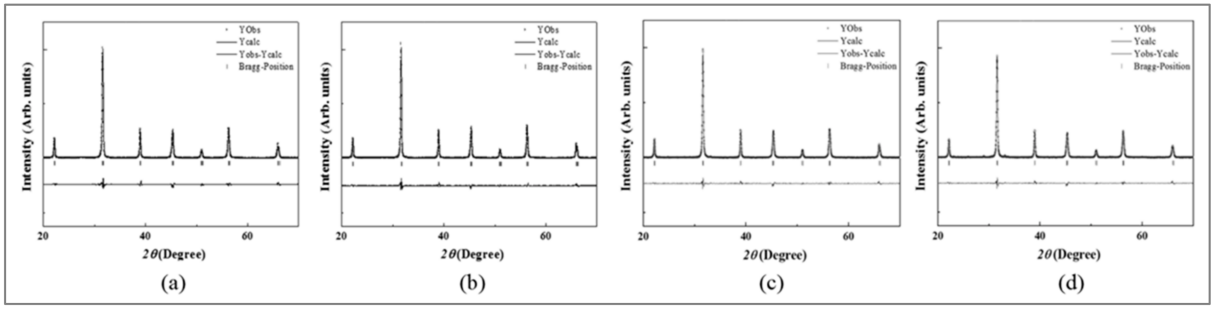

Figure 5. Rietveld refinement patterns of the 0.1 wt.% Dy_2O_3-doped $0.98BaTiO_3$-$0.02(Ba_{0.5}Ca_{0.5})SiO_3$ specimens sintered at 1320 °C for 1 h with various types of binders: (**a**) binder A, (**b**) binder B, (**c**) binder C, and (**d**) binder D.

Table 4. Refined structural parameters of the 0.1 wt.% Dy_2O_3-doped 0.98$BaTiO_3$-0.02($Ba_{0.5}Ca_{0.5}$)SiO_3 specimens sintered at 1320 °C for 1 h with different binders.

Composition	a and b (Å)	c (Å)	Unit Cell Volume (Å^3)	Tetragonality (c/a)	Goodness of Fit	Bragg R-Factor
No binder	3.9946	4.0115	64.0108	1.00423071	1.2	2.41
Binder A added specimen	3.9946	4.0116	64.0124	1.00425575	1.2	2.58
Binder B added specimen	3.9948	4.0116	64.0188	1.00420547	1.2	2.83
Binder C added specimen	3.9948	4.0116	64.0188	1.00420547	1.2	2.62
Binder D added specimen	3.9949	4.0117	64.0236	1.00420536	1.2	2.62

As can be observed from Table 5, the specimens showed a relative density of more than 92% for all the binder compositions. A uniform and homogeneous microstructure was observed, and the grain size did not change significantly with the variation in the binder type. However, for the specimens prepared using binders C and D, pores were observed at the grain boundaries. These results can be attributed to the decrease in the viscosity and solubility of PVA-111 in the binder solution at high ethyl alcohol volume fractions, as shown in Table 1.

Table 5. Relative densities of the 0.1 wt.% Dy_2O_3–doped 0.98$BaTiO_3$-0.02($Ba_{0.5}Ca_{0.5}$) SiO_3 specimens with different binders.

Composition	Sintering Condition	Density (g/cm^3)	Theoretical Density (g/cm^3)	Relative Density
No binder	1320 °C 1 h	5.4853	6.0133	91.22%
Binder A added specimens		5.5514	6.0123	92.33%
Binder B added specimens		5.5836	6.0128	92.86%
Binder C added specimens		5.5421	6.0127	92.17%
Binder D added specimens		5.5415	6.0137	92.15%

3.2.2. Electrical properties

Figure 6 shows the relationship between the relative density and dielectric constant (*K*) of the 0.1 wt.% Dy_2O_3–doped 0.98$BaTiO_3$-0.02($Ba_{0.5}Ca_{0.5}$)SiO_3 specimens sintered at 1320 °C for 1 h with different binder solutions. It is well-known that the dielectric properties of barium titanate ceramics are affected by their microstructural characteristics [24–26]. The dielectric constant (*K*) of the specimens first increased with an increase in the ethyl alcohol fraction of the binder solution up to 40 vol.% (binder B) and then decreased. This can be attributed to the decrease in the viscosity and surface tension of the binder solvent with an increase in the ethyl alcohol volume fraction, which in turn, resulted in the generation of pores in the microstructure (Figure 7) and a decrease in the relative density of the specimens (Table 5) [25].

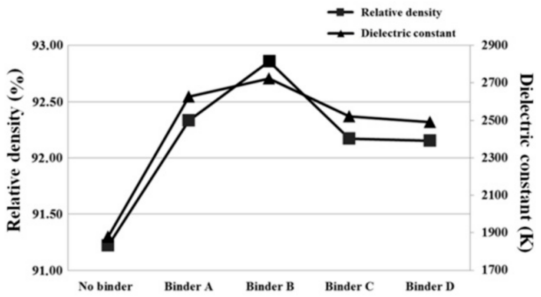

Figure 6. Relative densities and dielectric constants of the 0.1 wt.% Dy_2O_3-doped 0.98$BaTiO_3$-0.02($Ba_{0.5}Ca_{0.5}$)SiO_3 specimens sintered at 1320 °C for 1 h with different binders.

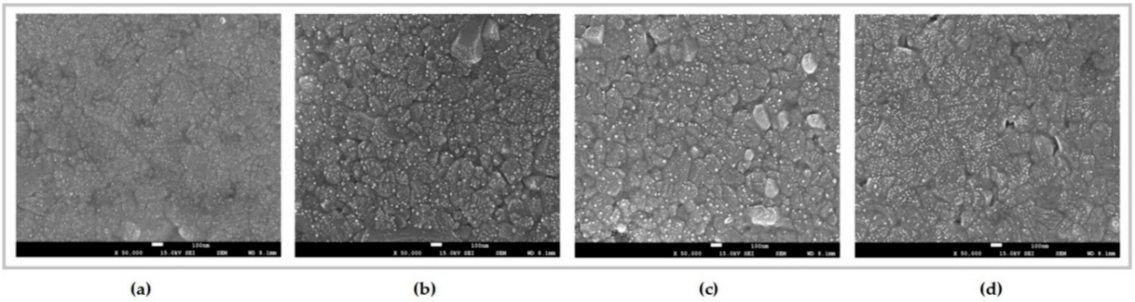

Figure 7. SEM images of the 0.1 wt.% Dy_2O_3-doped 0.98$BaTiO_3$-0.02($Ba_{0.5}Ca_{0.5}$)SiO_3 specimens sintered at 1320 °C for 1 h with various types of binders: (**a**) binder A, (**b**) binder B, (**c**) binder C, and (**d**) binder D (bar: 100 nm).

The dependence of the insulation resistance (IR) of the 0.1 wt.% Dy_2O_3-doped 0.98$BaTiO_3$-0.02($Ba_{0.5}Ca_{0.5}$)SiO_3 specimens sintered at 1320 °C for 1 h on their relative density is shown in Figure 8. As the microstructure of the sintered specimens could be controlled by varying the solvent composition of the binder solution, the insulation resistance of the specimens prepared using binder B increased to 270 GΩ (500 V, 60 s), while the dissipation factor (tanδ) decreased to 0.585. The IR and dissipation factor (tanδ) of the specimens were affected not only by the microstructural homogeneity, but also by their uniform grain size, which resulted from the uniform sintering reaction with the optimal composition of the binder solvent (binder B).

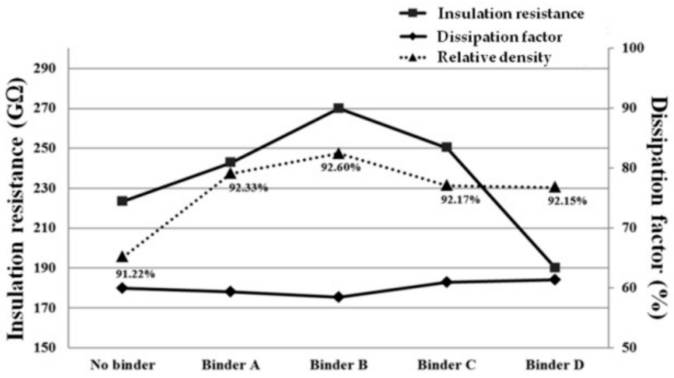

Figure 8. Insulation resistances, dissipation factors (tanδ), and relative densities of the 0.1 wt.% Dy_2O_3-doped 0.98$BaTiO_3$-0.02($Ba_{0.5}Ca_{0.5}$)SiO_3 specimens sintered at 1320 °C for 1 h with different binders.

4. Conclusions

The effect of the solvent composition of the PVA binder on the microstructure and electrical properties of the Dy_2O_3–doped 0.98$BaTiO_3$-0.02($Ba_{0.5}Ca_{0.5}$)SiO_3 ceramics ($0.0 \leq x$ wt.% ≤ 0.3) was investigated by varying the volume ratio of ethyl alcohol to distilled water in the PVA binder solvent. When no binder solution was used, the specimens sintered at 1320 °C for 1 h in a reducing atmosphere (95% N_2, 5% H_2) showed a $BaTiO_3$ single phase with the perovskite structure, irrespective of the Dy_2O_3 content (x wt.%) ($0.0 \leq x \leq 0.3$). The highest dielectric constant (K = 1878.5) and improved dissipation factor (tanδ = 0.60) were obtained for the 0.98$BaTiO_3$-0.02($Ba_{0.5}Ca_{0.5}$)SiO_3 specimens doped with 0.1 wt.% Dy_2O_3.

When the sintering was carried out at 1320 °C for 1 h, the 0.1 wt.% Dy_2O_3-doped 0.98$BaTiO_3$-0.02($Ba_{0.5}Ca_{0.5}$)SiO_3 specimens prepared using the PVA binder solution (ethyl alcohol/water = 40/60 v/o) showed higher dielectric constant (K = 2723.3) than the specimens prepared by the conventional solid-state reaction without a binder solution (K = 1878.5). This is because the PVA binder solution improved the microstructural uniformity of the specimens by improving the reactivity of the ceramic powder at the grain boundaries. In addition, the IR of the specimens increased from 223.5 to 270.0 GΩ and the

dissipation factor (tanδ) decreased from 0.6 to 0.585 when the optimal PVA binder solution composition (ethyl alcohol/water = 40/60 v/o) was used because of the improved relative density and microstructural uniformity of the sintered specimens.

Author Contributions: E.-S.K. and N.-B.J. designed the experiments. N.-B.J. and J.-S.B. performed the experiments and analysed the specimens. N.-B.J. analysed and explained the dependence of electrical properties on microstructure behaviours of the specimens. All the authors discussed the data and wrote the manuscript. All authors have read and agreed to the published version of the manuscript.

Funding: This work was supported by the Technology Innovation (20010938, development of 630V high capacity MLCC array module for power train), funded by the Ministry of Trade, Industry & Energy (MOTIE, Sejong City, Republic of Korea).

Institutional Review Board Statement: Not applicable.

Informed Consent Statement: Not applicable.

Data Availability Statement: Not applicable.

Acknowledgments: A part of this work was also supported by Kyonngi University's Graduate Research Assistantship 2021, Republic of Korea.

Conflicts of Interest: The authors declare no conflict of interest.

References

1. Pu, Y.; Chen, W.; Chen, S.; Langhammer, H.T. Microstructure and dielectric properties of dysprosium-doped barium titanate ceramics. *Ceramica* **2005**, *51*, 214. [CrossRef]
2. Kishi, H.; Kohzu, N.; Sugino, J.; Oshato, H.; Iguchi, Y.; Okuda, T. The effect of rare-earth (La, Sm, Dy, Ho and Er) and Mg on the microstructure in $BaTiO_3$. *J. Eur. Ceram. Soc.* **1999**, *19*, 1043. [CrossRef]
3. Mizuno, Y.; Kishi, H.; Ohnuma, K.; Ishikawa, T.; Oshato, H. Effect of site occupancies of rare earth ions on electrical properties in Ni-MLCC based on $BaTiO_3$. *J. Eur. Ceram. Soc.* **2007**, *27*, 4017. [CrossRef]
4. Han, Y.; Appleby, J.B.; Smith, D.M. Defects chemistry of $BaTiO_3$ with additions of $CaTiO_3$. *J. Am. Ceram. Soc.* **1987**, *70*, 100.
5. Chan, H.M.; Harmer, M.R.; Smith, D.M.L. Compensating defects in highly donor-doped $BaTiO_3$. *J. Am. Ceram. Soc.* **1986**, *69*, 507–510. [CrossRef]
6. Sato, T.; Shimada, M. Transformation of yttria-doped tetragonal ZrO_2 polycrystals by annealing in water. *J. Am. Ceram. Soc.* **1985**, *68*, 356. [CrossRef]
7. Zhao, Q.; Gong, H.; Wang, X.; Luo, B.; Li, L. Influence of BaO-CaO-SiO_2 on dielectric properties and reliability of $BaTiO_3$-based ceramics. *Phys. Status Solidi A* **2016**, *213*, 1077–1081. [CrossRef]
8. Miao, H.; Dong, M.; Tan, G.; Pu, Y. Doping effects Dy and Mg on BaTiO11 ceramics prepared by hydrothermal method. *J. Electroceram.* **2006**, *16*, 297–300. [CrossRef]
9. Yamaji, A.; Enomoto, Y.; Kinoshita, K.; Murakami, T. Preparation, characterization, and properties of Dy-doped small grained $BaTiO_3$ ceramics. *J. Am. Ceram. Soc.* **1977**, *60*, 97–101. [CrossRef]
10. Iwata, N.; Mori, T. Effect of binder addition on optimum additive amount of dispersant for aqueous $BaTiO_3$ slurry. *Ceram. Int.* **2019**, *45*, 19644–19649. [CrossRef]
11. de Laat, A.W.M.; Derks, W.P.T. Colloidal stabilization of $BaTiO_3$ with poly(vinyl alcohol) in water. *Colloids Surf. A Physicochem. Eng. Asp.* **1993**, *71*, 147–153. [CrossRef]
12. Li, C.C.; Lee, Y.C.; Cheng, Y.M. Effects of interactions among $BaTiO_3$, PVA, and B_2O_3 on the rheology of aqueous $BaTiO_3$ suspensions. *J. Am. Ceram. Soc.* **2010**, *93*, 3049–3051. [CrossRef]
13. Chen, H.; Wang, J.; Yin, X.; Xing, C.; Li, J.; Qiao, H.; Shi, F. Hydrothermal synthesis of $BaTiO_3$ nanoparticles and role of PVA concentration in preparation. *Mater. Res. Express* **2019**, *6*, 055028. [CrossRef]
14. Paik, U.; Hackley, V.A.; Lee, J.; Lee, S. Effect of poly(acrylic acid) and poly(vinyl alcohol) on the solubility of colloidal $BaTiO_3$ in an aqueous medium. *J. Mater. Res.* **2003**, *18*, 5. [CrossRef]
15. Iijima, M.; Sato, N.; Lenggoro, I.W.; Kamiya, H. Surface modification of $BaTiO_3$ particle by silane coupling agents in different solvent and their effect on dielectric properties of $BaTiO_3$/epoxy composites. *Colloids Surf. A Physicochem. Eng. Asp.* **2009**, *352*, 88–93. [CrossRef]
16. Khattab, I.S.; Bandarker, F.; Fakhree, M.A.A.; Jouyban, A. Density, viscosity, and surface tension of water+ethanol mixture from 293 to 323K. *Kor. J. Chem. Eng.* **2012**, *29*, 812–817. [CrossRef]
17. Hassan, C.M.; Trakampan, P.; Peppas, N.A. Water solubility characteristics of poly(vinyl alcohol) and gel prepared by freezing/thawing process. In *Water Soluble Polymers*; Springer: Boston, MA, USA, 2002; pp. 31–40.
18. DeVries, R.C.; Roy, R. Phase Equilibria in the System $BaTiO_3$-$CaTiO_3$. *J. Am. Ceram. Soc.* **1955**, *38*, 142–146. [CrossRef]

19. Makovec, D.; Samardzija, Z.; Drofenik, M. Solid solubility of holmium, yttrium, and dysprosium in $BaTiO_3$. *J. Am. Ceram. Soc.* **2004**, *87*, 1324–1329. [CrossRef]
20. Kingery, W.D.; Bowen, H.K.; Uhlmann, D.R. (Eds.) *Introduction to Ceramics*, 2nd ed.; Wiley: New York, NY, USA, 1976; pp. 913–974.
21. Feng, T.T.; Hsieh, H.L.; Shiau, F.S. Effects of pore morphology and grain size on the dielectric properties and tetragonal-cubic phase transition of high-purity barium titanate. *J. Am. Ceram. Soc.* **1993**, *76*, 1205–1211. [CrossRef]
22. Lee, E.J.; Jeong, J.; Han, Y.H. Defects and degradation of $BaTiO_3$ codoped with Dy and Mn. *Jpn. J. Appl. Phys.* **2006**, *45*, 822–825. [CrossRef]
23. Lee, E.J.; Jeong, J.; Han, Y.H. Electrical properties of Dy_2O_3-doped $BaTiO_3$. *Jpn. J. Appl. Phys.* **2004**, *43*, 8126. [CrossRef]
24. Barzic, A.I.; Stoica, I.; Brazic, R.F. Microstructure implications on surface features and dielectric properties of nanoceramics embedded in polystyrene. *Rev. Roum. Chim.* **2015**, *60*, 809–815.
25. Maiwa, H. Dielectric and electromechanical properties of $Ba(Zr_xTi_{1-x})O_3$ (x = 0.1 and 0.2) ceramics prepared by spark plasma sintering. *J. Appl. Phys.* **2007**, *46*, 7013. [CrossRef]
26. Hoshina, T.; Takizawa, K.; Li, J.; Kasama, T.; Kakemoto, H.; Tsurumi, T. Domain size effect on dielectric properties of barium titanate ceramics. *J. Appl. Phys.* **2008**, *47*, 7607. [CrossRef]